INSTITUT FÜR INFORMATIK

UND PRAKTISCHE MATHEMATIK

Approximate Orientation Steerability
Based on Angular Gaussians

Weichuan Yu, Kostas Daniilidis, Gerald Sommer

PAX OPTIMA RERUM

CHRISTIAN-ALBRECHTS-UNIVERSITÄT

KIEL

Institut für Informatik und Praktische Mathematik der
Christian-Albrechts-Universität zu Kiel
Olshausenstr. 40
D – 24098 Kiel

Approximate Orientation Steerability Based on Angular Gaussians

Weichuan Yu, Kostas Daniilidis, Gerald Sommer

e-mail: {wy,gs}@ks. informatik.uni-kiel.de

The address of K. Daniilidis is: GRASP Lab, University of
Pennsylvania, Philadelphia, PA 19104-6228, USA.
e-mail: kostas@grip.cis.upenn.edu.

Approximate Orientation Steerability Based on Angular Gaussians

Weichuan Yu, Kostas Daniilidis, Gerald Sommer

9. November 1999

Abstract

Junctions are significant features in images with an intensity variation that exhibits multiple orientations. This makes the detection and characterization of junctions a challenging problem. In this work, we deal with the characterization of junctions which would ideally be the response of a filter at every orientation. This can be achieved by the principle of steerability that enables the decomposition of a filter into a linear combination of basis functions. However, current steerability approaches suffer from the consequences of the uncertainty principle: In order to achieve high resolution in orientation they need a large number of basis filters increasing, thus, the computational complexity. Furthermore, these functions have usually a wide support which only accentuates the computational burden.

In this report we propose a novel alternative to current steerability approaches. It is based on utilizing a set of polar separable filters with small support to sample orientation information. The orientation signature is then obtained by interpolating orientation samples using Gaussian functions with small support. Compared with current steerability techniques our approach achieves a higher orientation resolution with a lower complexity. In addition, by observing that the orientation scale of a filter is inversely proportional to its orientational bandwidth, we build a polar pyramid to characterize junctions of arbitrary inherent orientation scales.

1 Introduction

Junctions of gray-value lines or edges in images carry important information for many image processing tasks like point matching in object recognition, point tracking in motion analysis, attentive coding, and line-drawing interpolation [17]. In order to use junctions for such tasks we must be able to localize their corresponding keypoints which are defined as intersection points of lines or edges. Then, we must characterize junctions by means of signatures and classify them in junction categories. Regarding keypoint detection and localization the reader is referred to Foerstner's study [9] and the work of Parida et al. [11] and to the comparison of different operators by Rohr [21, 22]. In this report we address the problem of junction characterization. The resulting signature can be used for further junction classification.

Junctions are local structures with multiple intrinsic orientations and spatial scales [2]. For the purpose of characterization we project them onto the orientation space and build a 1D signature function of the orientation parameter. Such signatures are often obtained by applying a set of filters at different orientations. This leads to an enormous computational load. For example, in order to extract orientation information of a junction, with conventional filter methods we have to rotate the same filter around the keypoint repeatedly. For an angular field of $360°$ and a sampling interval of $5°$ already 72 rotated copies of the original filter should be applied. The concept of steerability has been introduced in order to reduce this explosion of computational complexity. Steerable filters obtain an analytic model of deformations for further analysis of the grey-value structure [7, 13, 10, 1, 4, 24, 20].

Denoting with α ($\alpha \in I\!R$) the deformation parameter we define a filter $F(\vec{x})$ with $\vec{x} \in I\!R^n$ as a steerable filter if its deformed versions $F_\alpha(\vec{x})$ can be expressed as [16]:

$$F_\alpha(\vec{x}) = \sum_{k=1}^{N} b_k(\alpha) A_k(\vec{x}), \tag{1}$$

where $A_k(\vec{x})$ and $b_k(\alpha)$ are referred to as basis filters and interpolation functions, respectively. The signature $S(\alpha)$ of a junction can be obtained by applying such a steerable filter on the image $I(\vec{x})$:

$$S(\alpha) \stackrel{def}{=} \langle F_\alpha(\vec{x})|I(\vec{x})\rangle = \sum_{k=1}^{N} b_k(\alpha)\langle A_k(\vec{x})|I(\vec{x})\rangle. \tag{2}$$

2

Here $\langle \cdot | \cdot \rangle$ denotes the usual inner product for two real functions $F(\vec{x})$ and $G(\vec{x})$:

$$\langle F(\vec{x}) | G(\vec{x}) \rangle \overset{def}{=} \int_{\vec{x}} F(\vec{x}) G(\vec{x}) \, d\vec{x}.$$

We see the motivation of steerability clearly in equation (2): The responses of the filter $F_\alpha(\vec{x})$ with $\alpha \in I\!R$ are expressed as a linear combination of N basis filter responses. According to our opinion, steerability approaches may be classified in exact and approximate methods.

Although steerability was implicitly used by Danielsson and Knutsson [7, 13], Freeman and Adelson [10] were the first who coined the concept and introduced an *exact* steerability approach. The approach of Freeman and Adelson to orientation steerability of a Gaussian derivative is an interpolation using harmonic functions in the orientation space given the fact that a filter is periodic with respect to orientation. The basis functions are rotated copies of the original filter. The derived kernels do not possess sufficient orientational resolution due to their large spatial support in orientation. Moreover, they are either symmetric or antisymmetric [23]. This results in a period of $180°$ in orientation and leads to an ambiguity in responses between terminating and non-terminating junctions.

Simoncelli et al. [1] extended this concept to include dilation and translation. They proposed some conditions upon which a filter is guaranteed to be exactly steerable, i.e. a filter can be synthesized with finite Fourier bases. Recently, Simoncelli and Farid [23] designed a steerable wedge filter in the opposite direction. Regarding the angular direction, they do not first choose one filter with expected shape and then project it onto the Fourier basis. Instead, they first choose finite components from the Fourier basis and then synthesize the filter *only* using these components. Therefore, their filter is guaranteed to be band limited and exactly steerable. Besides, the shape of the wedge filter can be adjusted to be arbitrarily narrow if we adopt adequate Fourier components. There is no more symmetric ambiguity applying a steerable wedge filter because the wedge kernel is asymmetric in the angular direction.

Michaelis and Sommer [16] and Teo and Hel Or [24] provided the formal justification of the exact steerability by applying Lie-group theory. The basic concept of exact steerability is the shiftability [1]: Every periodic band-limited function can be approximated at every position ("shift") with a finite linear combination of harmonic functions. In this sense, orientation and scaling become translations if we apply a logarithmic-polar transformation to a function with two arguments. Lie group theory gives us the theoretical framework for this transformation and for the exact interpolation. The complex harmonics $e^{j\omega k}$ are the generating operators of translation. On the other hand, all one-

3

parameter Lie groups are locally isomorphic to the translation group if we change the coordinates to so called canonical coordinates, for example, Cartesian to polar coordinates for rotations. Thus, for every deformation we achieve exact steerability if we transform the coordinates to canonical ones and then apply Fourier analysis. Teo and Hel Or list a complete classification of functions steerable with respect to any Abelian group.

Perona [19] introduced the concept of deformable kernels which is based on the minimization of the discrepancy between the left-hand side and the right-hand side of equation (1) with respect to the basis functions $A_k(\vec{x})$. He showed that the basis functions are the right singular functions of a continuous SVD. In case of rotations and periodic translations it can be proved [14] that the basis functions are the same in both the deformability and the exact Lie-group based steerability. However, for other deformations the functions must be sampled with respect to the deformation parameter and a numerical SVD is applied [12]. The advantage of the *deformability* approach is that it steers continuous and discrete filters and needs a minimal number of basis functions for a given error. However, orientational resolution is not addressed in this approach so that usually this approach suffers from the uncertainty constraint. Since we are interested only in orientation, both approaches yield the same set of basis functions. Therefore, from now on, we will use for both approaches to orientation steerability the term exact steerability.

The steerability problem may be also considered as a problem of signal reconstruction from samples $A_k(k = 1, \cdots, N)$ (see equation (1)). This becomes evident if we consider the parameter α in equation (1) to be the same as the spatial domain variable. For clarity we change the notation to θ:

$$f(\theta) = \sum_{k=1}^{N} A_k b_k(\theta). \tag{3}$$

Here the interpolation functions $b_k(\theta)$ can be from many function classes, for example Laguerre functions or Legendre polynomials ([18], pp. 29-30). In current orientation steerability approaches $b_k(\theta)$ are usually the complex harmonics $e^{j\omega_k\theta}$, yielding

$$f(\theta) = \sum_{k=1}^{N} A_k e^{j\omega_k\theta}. \tag{4}$$

Note that ω_k are not necessarily the first N frequencies as in the *standard* Fourier decompositions.

In this report,

4

- we point out that the exact approach to orientation steerability has insufficient orientational resolution because it is based on the sampling of the angular frequency. To achieve a high orientational resolution a huge number of filters must be used. Due to the uncertainty principle this computational burden is amplified by the large support of the basis functions.

- We will introduce a new approximation approach based on Gaussian functions which might be non-optimal with respect to the approximation error but substantially alleviates the above problems as shown in theory and experiments.

We extend this approach to an efficient hierarchical scheme and provide a complete analysis of computational complexity. Thus, by considering only the problem of orientation steerability, we sacrifice a coherent algebraic theory (as in Lie group and SVD-based deformability approaches) to achieve high orientational resolution as well as a dramatical decreasing of the computational complexity.

This report is organized as follows: In section 2 we introduce the new approximate steerability approach based on angular Gaussians and point out the theoretical difference between our approach and current steerability approaches. Besides, we analyze their computational complexity in detail. In section 3 we further introduce a polar pyramid scheme to treat orientation scale variations. Then we present experimental results on both synthetic and real data which vividly show a better performance of our approach. This report is concluded with a short discussion.

2 Approximate Orientation Steerability

2.1 Definition

A 1D continuous function $f(\theta)$ ($\theta \in I\!R$) can be approximated from samples as a linear combination of appropriate interpolation functions (see equation (3)). The main goal of our approach is high orientational resolution. Therefore, we are interested in filters with narrow support. We choose shifted Gaussians because they achieve the lower bound in the uncertainty principle:

$$b_k(\theta) = G_0(\theta - \theta_k) = \frac{1}{\sqrt{2\pi}\sigma} e^{-\frac{(\theta - \theta_k)^2}{2\sigma^2}}, \tag{5}$$

5

with θ_k distributed evenly along the axis of the orientation variable θ. We approximate the orientation response with an orientation signature $S(\theta)$ defined as follows:

$$f(\theta) \approx S(\theta) \stackrel{def}{=} \sum_{k=1}^{N} A_k b_k(\theta) = \sum_{k=1}^{N} A_k G_0(\mathcal{D}(\theta, \theta_k)), \tag{6}$$

where θ denotes the angular variable and $\theta_k (k = 1, \cdots, N)$ are evenly distributed angular values. Since θ and θ_k are circular angles ($\theta, \theta_k \in [0, 2\pi]$), we define a $\mathcal{D}(\cdot)$ to represent the minimal circular difference between θ and θ_k

$$\mathcal{D}(\theta, \theta_i) = min(|\theta - \theta_i|, |\theta - \theta_i - 2\pi|, |\theta - \theta_i + 2\pi|). \tag{7}$$

For example, $\mathcal{D}(2\pi, 0) = 0$; $\mathcal{D}((2\pi - \frac{\pi}{180}), \frac{\pi}{180}) = \frac{\pi}{90}$.

In the study of local orientation, we first conduct a local polar transformation from Cartesian to the polar coordinate system and we denote the new intensity function with $I(r, \theta)$, where r and θ are the radius and angle, respectively. Since we are merely interested in orientation, we eliminate the radial variable r by applying averaging along the radial direction. We denote inner and outer boundaries of the polar transformation with $R_{\min}$ and $R_{\max}$, respectively (see figure 1). We set $R_{\min} > 0$ to avoid the singularity close to the keypoint [15]. In order to choose $R_{\max}$ we must know the size of the significant neighborhood around the keypoint, which can be provided by the preceding keypoint detection step. In this report we set $R_{\min} = 3$ pixels and $R_{\max}$ varies from 9 to 15 pixels.

To achieve the approximation properties with respect to the angle we choose sample positions θ_k as described later and take the scalar product of the intensity with the Gaussian:

$$A_k = \sum_{\theta = \theta_k - \frac{W}{2}}^{\theta_k + \frac{W}{2}} G_0(\mathcal{D}(\theta, \theta_k)) \sum_{r=R_{\min}}^{R_{\max}} \frac{1}{\mathcal{N}(R_{\min}, R_{\max}, \theta_k)} I(r, \theta), \tag{8}$$

where $\mathcal{N}(R_{\min}, R_{\max}, \theta_k)$ is an averaging factor along the radial direction which is the sum of discrete weights inside the sampling mask centered at θ_k. The inner sum averages over the radius by normalizing with $\mathcal{N}(R_{\min}, R_{\max}, \theta_k)$. The outer sum is the projection of the shifted angular Gaussian on the angular signal. Theoretically, a Gaussian function is not compactly supported. In practice we only consider the part of $G_0(\mathcal{D}(\theta, \theta_k))$ whose variable varies from $\theta_k - \frac{W}{2}$ to $\theta_k + \frac{W}{2}$. Here W denotes the angular width of the sampling mask. In figure 1 we show a sampling mask centered at θ_k. We will explain the choice of this parameter in section 2.3. If we consider A_k in equation (6) as basis filter responses we have introduced an *approximate steerability* which reconstructs *continuous* $S(\theta)$ using Gaussian interpolation functions.
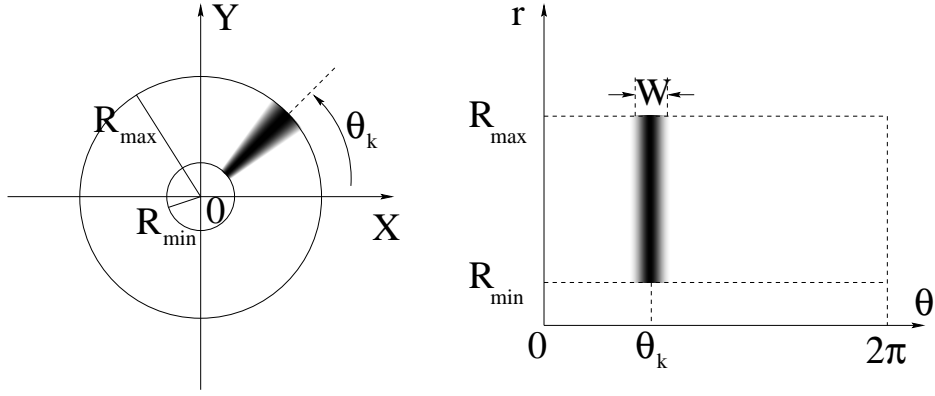
6

Figure 1: A Gaussian averaging mask centered at angle θ_k. Darker pixels represent larger gray values. **Left:** The mask in the Cartesian coordinate system. The keypoint is at the center of the circle. **Right:** The mask with r and θ as coordinates, $R_{\max}$ and $R_{\min}$ are radial boundaries of the mask, W is the angle width of the mask. We set $R_{\min} > 0$ to avoid the confusion close to the keypoint.

In the orientation signature $S(\theta)$ local extremes represent orientations of lines and the positions of steepest descent/ascent indicate orientations of edges. Correspondingly, the 2D orientation analysis reduces into 1D line/edge detection. In order to extract edge information we estimate the derivative of $S(\theta)$:

$$
\begin{aligned}
DS(\theta) \quad &\overset{def}{=} \quad |\frac{d}{d\theta}S(\theta)| \\
&= \quad |\sum_{k=1}^{N} A_k \frac{d}{d\theta}G_0(\mathcal{D}(\theta,\theta_k))| \\
&= \quad |\sum_{k=1}^{N} A_k G_1(\mathcal{D}(\theta,\theta_k))|,
\end{aligned}
\tag{9}
$$

where $G_1(\mathcal{D}(\theta,\theta_k))$ denotes the first derivative of Gaussian filter G_0 and $|\cdot|$ denotes the absolute value. Here, we are only interested in the amplitude of the derivative. We point out here that though $S(\theta)$ and $DS(\theta)$ seem similar to the even and the odd responses of a quadratic filter, it is not suitable to combine them together as a single energy response since they are not Hilbert transformations of each other. To accomplish junction classification, both information on lines and edges is necessary. In case of a quadrature filter, the magnitude signature would not suffice, and we would need odd/even or magnitude/phase signatures to characterize a junction.

So far, we have defined the approximate steerability. In the following we will compare

this approach with current steerability approaches regarding the mathematical background and the implementation performance.

2.2 Difference to Exact Steerability

The main difference between our approach and the exact steerability is that we decompose one signal *locally* in the spatial domain, whereas exact approaches decompose the signal *globally*. This difference lies in both the basis filters and the interpolation functions: In order to calculate the response of a basis filter (i.e. A_k in equation (4) and in equation (6)) we need a Gaussian mask with local spatial support in the approximate steerability (as shown in figure 1), while in the exact steerability every basis filter has the same wide spatial support as the steered filter.

This difference can be described in the spectral domain as well. In the approximate steerability (equation (6)) the spectrum of one signal is decomposed into a set of *spectral* Gabor functions (Gaussian functions with different locations) weighted by the averaging outputs:

$$
\begin{aligned}
\mathcal{F}[S(\theta)] \;\; &\overset{def}{=} \;\; \sum_{k=1}^{N} A_k \mathcal{F}[G_0(\theta - \theta_k)] \\
&= \;\; \sum_{k=1}^{N} A_k \mathcal{F}[G_0(\theta)] e^{-j\omega\theta_k},
\end{aligned}
\tag{10}
$$

where $\mathcal{F}$ denotes the Fourier transform. In contrast, in the exact steerability (equation (4)) the spectrum of one signal is decomposed into a series of Dirac sampling functions weighted by the corresponding basis filter responses:

$$
\mathcal{F}[f(t)] = \sum_{k=1}^{N} A_k \delta(\omega - \omega_k).
\tag{11}
$$

Thus, in the case of approximate steerability we sample the signal in the spatial domain with Gaussian masks whereas in the exact steerability the signal is sampled in the spectral domain by Dirac sampling functions. This difference makes our approach perform better with respect to orientational resolution. According to the well known uncertainty principle, we cannot localize one signal both in the spatial domain and in the spectral domain exactly. If we use one Dirac sampling function to localize one spectral component of the signal exactly, as in the case of the exact orientation steerability, we will no

8

more be able to localize this component in the spatial domain. Therefore, we need many Dirac impulses to increase the localization capability in space. This trade-off can be optimized by applying functions with Gaussian shape [8]. Therefore, the approximate steerability has better properties with respect to the uncertainty principle.

To summarize, our main concern is orientational resolution with low complexity. To achieve this goal, we directly built our filter in the spatial domain. The price we pay is that we do not achieve exact steerability but an approximation of the orientation response.

2.3 Complexity Analysis

Approximate steerability tries to achieve a higher orientation resolution with a lower complexity due to the narrow support of the basis filters. Our approach starts with a local polar mapping which can be done "off-line" since it is a transform between coordinates and is therefore valid for *all* different images. Online applying the resulting look-up-table (LUT) is of negligible complexity compared with calculating the filter responses.

In order to compare the implementation complexity of the approximate steerability and that of the exact approach we set the radial extensions of masks in both schemes to be the same. If we denote the 1D tap size of an exactly steerable filter with P, the following relation is satisfied:

$$P = 2R_{\max} + 1.$$

Here, we choose the steerable wedge filter [23] for comparison since it has the similar shape to our filter mask. The steerable wedge filter is a separable polar filter. Its radial component looks like a wedge and its angular component is synthesized by the Fourier series. Its computational complexity is proportional to the number and the spatial support of basis filters. In order to make a fair comparison we apply it after the local polar mapping, too. It should be noticed that polar separability is not an advantage for calculating the inner product, since the complexity of the scalar product remains P^2 multiplications and $P^2 - 1$ additions. Polar separability could be exploited only if we could perform a convolution.

Suppose we apply a steerable wedge filter composed of $2N$ basis filters (N odd basis filters and N even basis filters). As mentioned before, all basis filters have the same spatial support as the steered filter, the 1D size of all basis filters is therefore P, too. In order to apply one basis filter we need P^2 multiplications and $P^2 - 1$ additions to calculate the

9

corresponding inner product. Straightforwardly, $2NP^2$ multiplications and $2N(P^2-1)$ additions are required to obtain $2N$ coefficients (see equation (2)). Assuming that we use signatures of length 360 we need $720N$ multiplications and $720(N-1)$ additions to obtain outputs of odd and even filters. Thus, totally $2N(P^2+360)$ multiplications and $2N(P^2+359)$ additions are computed to implement a steerable wedge filter composed of N odd basis filters and N even basis filters.

The main factors in our approach are the number and the width of Gaussians. To satisfy the Nyquist rate in the sampling theory we require following relation between the sampling interval $\delta\theta$ and the Nyquist frequency f_m:

$$\delta\theta \leq \frac{1}{2f_m}. \tag{12}$$

For example, we should set the sampling interval $\delta\theta \leq 1°$ if we want to keep orientational frequencies below $f_m = \frac{90}{\pi} \approx 28(Hz)$. Totally we need $N = \frac{360}{\delta\theta}$ basis filters to sample the whole orientation space.

The angular width of the sampling mask W is related to the scale of the Gaussian function σ. Here, instead of applying Dirac sampling functions along the angular direction we use Gaussian masks. This is equivalent to Dirac series (the shah function $III(\theta)$ [5]) convolved with a Gaussian function. Correspondingly, the spectrum of the ideal sampling will be further multiplied by a low pass filter with Gaussian shape. The stop frequency of this low pass filter is determined by the term $\frac{1}{2\sigma}$ (here we define the turning frequency of the Gaussian function $\frac{1}{2\sigma}$ as the stop frequency). This stop frequency is preferred to be not below the Nyquist frequency f_m:

$$\frac{1}{2\sigma} \geq f_m, \quad \text{hence} \quad \sigma \leq \frac{1}{2f_m}. \tag{13}$$

On the other hand, the filter mask should contain adequate pixels to calculate averaging values robustly. Therefore, we set $\sigma = \delta\theta$. Since we want to use the Gaussian function as an FIR-filter we must cut off its support. It is easy to show that in order to keep the energy of the cut-off area below 1% of the total energy the width of the mask must be at least 5σ. In this report, we set $W = 6\sigma$.

We use $N = \frac{360}{\delta\theta}$ sampling masks to obtain angular samples $A_k (k = 1, \cdots, N)$. On an average we have at most $\frac{W}{360}\pi(R_{\max}^2 - R_{\min}^2) < \frac{W}{360}P^2$ pixels in one sampling mask. For simplicity we assume that in one sampling mask there are $\frac{W}{360}P^2$ pixels. Correspondingly, we need $\frac{W}{360}P^2$ multiplications and $\frac{W}{360}P^2 - 1$ additions to calculate one angular sampling. Taking into account that $W = 6\delta\theta$ we need $6P^2$ multiplications and $6P^2 - \frac{360}{\delta\theta}$ additions to obtain N samples. In constructing $S(\theta)$ or $DS(\theta)$ we apply a

10

Gaussian function and its first derivative, respectively, with the angular width W as interpolation functions. In order to produce the signatures $S(\theta)$ and $DS(\theta)$ with the same length of 360 as in the wedge filter approach above, we require $360W$ multiplications and $360(W-1)$ additions for interpolation. Thus, totally we need $6P^2 + 4320\delta\theta$ multiplications and $6P^2 + 4320\delta\theta - \frac{360}{\delta\theta} - 720$ additions to obtain $S(\theta)$ and $DS(\theta)$ in case of approximate steerability.

The complexity of both approaches is plotted in figure 2. In the approximate steerability the sampling interval $\delta\theta$ plays a very interesting role. We observe that by setting $\delta\theta$ smaller, which means we have higher orientation resolution, computation load decreases. We can draw the conclusion that the approximate steerability is more efficient than the exact steerability, especially in the case of high orientation resolution and large filter size.

3   Junction Characterization Using a Polar Pyramid

The orientation scale problem is like every scale problem a trade-off between the intrinsic structure of a junction and the orientation scale of a filter. As shown in figure 9, if the orientation scale of a filter is too small, a blurred edge is not visible and a wide line will be recognized as two edges [15]. If the orientation scale of a filter is too large, two very close lines will be characterized as one line. In this section we introduce a polar pyramid to obtain signatures of different scales efficiently. Here we do not treat the problem of steering spatial scale. Regarding the steerability of spatial scale the reader is referred to [20, 14].

It is known that one of the most appealing kernels for hierarchical approaches is the Gaussian function [3]. We know from spatial scale theory that the choice of scale necessitates a hierarchical treatment. Burt and Adelson [6] prove that a generating kernel of subsampling can be used as the interpolation function for reconstruction from coarser scales. Moreover, they argue that the interpolation functions can be (discrete approximations of) Gaussian functions with different scales (figure 3). Thus, the continuous orientation information can be reconstructed from all levels of the polar pyramid by interpolating the pyramid elements $\hat{S}^j(\theta)$ with Gaussian functions $G^j(\theta)$ of different scales σ_j :

$$S^j(\theta) = \sum_n \delta(\theta - n\triangle\theta)\hat{S}^j(\theta) * G_0^j(\theta) \qquad j \in [1, 2, \cdots] \tag{14}$$

11

with

$$G_0^j(\theta) = \frac{1}{\sqrt{2\pi}\sigma_j} e^{-\frac{\theta^2}{2\sigma_j^2}} \qquad j \in [1, 2, \cdots], \tag{15}$$

where $\hat{S}^j(\theta)$ denote the elements on the j-th level of the polar pyramid and $S^j(\theta)$ represents the signature reconstructed from $\hat{S}^j(\theta)$. We can obtain edge signatures similarly:

$$DS^j(\theta) = | \sum_n \delta(\theta - n\triangle\theta)\hat{S}^j(\theta) * G_1^j(\theta) | \qquad j \in [1, 2, \cdots], \tag{16}$$

where $G_1^j(\theta)$ is the first derivative of $G_0^j(\theta)$. The local maxima in $S^j(\theta)$ and $DS^j(\theta)$ denote orientations of lines and edges at different scales, respectively.

If we want to build a pure 1D one-octave Gaussian pyramid of angles, according to [6] we should have $M2^L + 1$ samples where L is the number of levels and $M + 1$ is the number of samples at the highest level. Taking the periodicity into account we should have $M2^L$ samples as the sampling outputs. However, since initially the orientation signal is defined as 360 discrete values we cannot build a pure octave Gaussian pyramid. Alternatively, we apply a factor 2 subsampling of the first three levels, a factor 3 at the next two, and have 5 samples at the coarsest level ($360 = 2^3 \times 3^2 \times 5$). Let us denote with $K_i(j)$ the j-th coefficient of the FIR filter in the i-th pyramid layer. According to [6] the generating kernels with subsampling factor i should be normalized

$$\sum_{j=1}^{2i+1} K_i(j) = 1 \qquad i \in [2, \cdots] \tag{17}$$

and symmetric

$$K_i(j) = K_i(2i + 1 - (j - 1)) \qquad j \in [1, \cdots, i + 1]. \tag{18}$$

Moreover, every sample at a given level should make equal contributions to construct the next higher level. The contributions of one sample are weighted by the corresponding coefficients of the generating kernels. Equal contributions imply that the sum of all its connected elements in the generating kernels should be a constant.

As mentioned in [6], the generating kernels satisfying the above constraints should have Gaussian shape. We use the following discrete approximations of Gaussian functions to serve as generating kernels with subsampling factor 2, 3 and 5:

$$K_2 = \frac{1}{16} \begin{pmatrix} 1 & 4 & 6 & 4 & 1 \end{pmatrix}, \tag{19}$$

12

$$K_3 = \frac{1}{264} \begin{pmatrix} 3 & 22 & 66 & 82 & 66 & 22 & 3 \end{pmatrix}, \tag{20}$$

$$K_5 = \frac{1}{5120} \begin{pmatrix} 1 & 74 & 299 & 725 & 950 & 1022 & 950 & 725 & 299 & 74 & 1 \end{pmatrix}. \tag{21}$$

4 Experiments

4.1 Synthetic Junction Examples

In this section we illustrate some examples of junction characterization using the approximate steerability and its hierarchical version. In figures 4 and 5 synthetic line junctions and edge junctions are shown, respectively. The corresponding signatures $S(\theta)$ and $DS(\theta)$ characterize them correctly. The small deviations in figure 5 come from the fact that an edge can only be represented by two pixels in the grid, while we cannot set the center of a wedge between two pixels.

The robustness of our method against noise is shown in figure 6. The edge junction is disturbed with increasing random noise. Even in the very noisy case the junction is well characterized. The keypoints in figure 7 are deviated from the central positions of the masks. Though the signatures have some variations, we can still characterize the junctions.

In figure 8 we compare the performance of both steerability approaches. A complex junction called "Siemens star" with 16 edges spans the orientation space uniformly. Applying the steerable wedge filter we even have to use 90 basis filters to achieve the same orientation resolution as applying the Gaussian averaging steerable filter. Hence, we need about eleven times as many multiplications and thirteen times as many additions using the steerable wedge filter as using the Gaussian averaging steerable filter. This demonstrates the advantages of the local decomposition scheme in the approximate steerability.

Figure 9 is an example to solve the orientation scale problem applying a polar pyramid. The junction is composed of two blurred edges, a wide line and two close lines. We use a polar pyramid with four levels to characterize it. With the increase of the pyramid level the orientation of the wide line and blurred edges are characterized more and more distinctly. However, in the mean time the responses of two close lines seem more and more like one line. This is exactly the demonstration of orientation scale problem.

13

4.2 Real Experiments

We have observed the successful behavior of the approximate steerability on synthetic junction characterizations. Here we show some real experimental results. One example is the parkbench picture used in [23] (figure 10). In comparison to the steerable wedge filter [23] with 30 basis filters our method characterizes the directions of junctions more distinctively. This is explicitly presented by the 'T' junction in **D** where the blurred edge near $180°$ is better characterized with the approximately steerable filter. We see also that our approach is relatively more sensitive to high frequency components due to the differentiation.

Another real example is presented in figure 11. The kernel centers are displaced from the keypoints of the junctions. The results show that both steerable wedge filter and approximately steerable filter are stable with respect to the offsets of keypoints while the Gaussian approach achieves higher orientation resolution with lower cost.

In figure 12 we show the high orientation resolution of the approximate steerability. While the steerable wedge filter [23] with 90 basis filters only detects the dominant dark line between the lips of Lena, the approximately steerable filter characterizes edges of two lips distinctly. This may be very useful in facial feature analysis.

A real example with varying scales is further presented in figure 13. A child's left eye corner can be regarded as a combination of irregular wide lines and blurred edges disturbed by noise. The characterizing results from different pyramid levels form a complete set of signatures providing information at different orientation scales.

5 Conclusion

Current orientation steerability approaches are based on the Fourier decomposition of the steered filter with respect to orientation. Although they are optimal with respect to approximation error, they suffer from the uncertainty principle: Due to the sampling of the spectral domain with Dirac functions the filters have wide spatial supports. In order to achieve high orientational resolution a huge number of basis filters must be applied.

We proposed a new approach to obtain the orientation signature for junction characterization. We called it approximate steerability because it enables the approximation of a continuous response with respect to orientation based on a number of basis filter responses. These filters are directly designed in the spatial domain to have narrow support. We use Gaussian functions of 0-th and 1st order to characterize lines and edges,

respectively. Because we are interested in the discrimination of lines from edges we did not use a quadrature pair. The narrow support of the basis functions enables a high orientational resolution with a moderate computational load. We showed this difference to earlier approaches both in theory as well as in real images of junctions. In the next report we will extend this approximate steerability to 3D filtering and display their applications in 3D image processing.

Acknowledgment
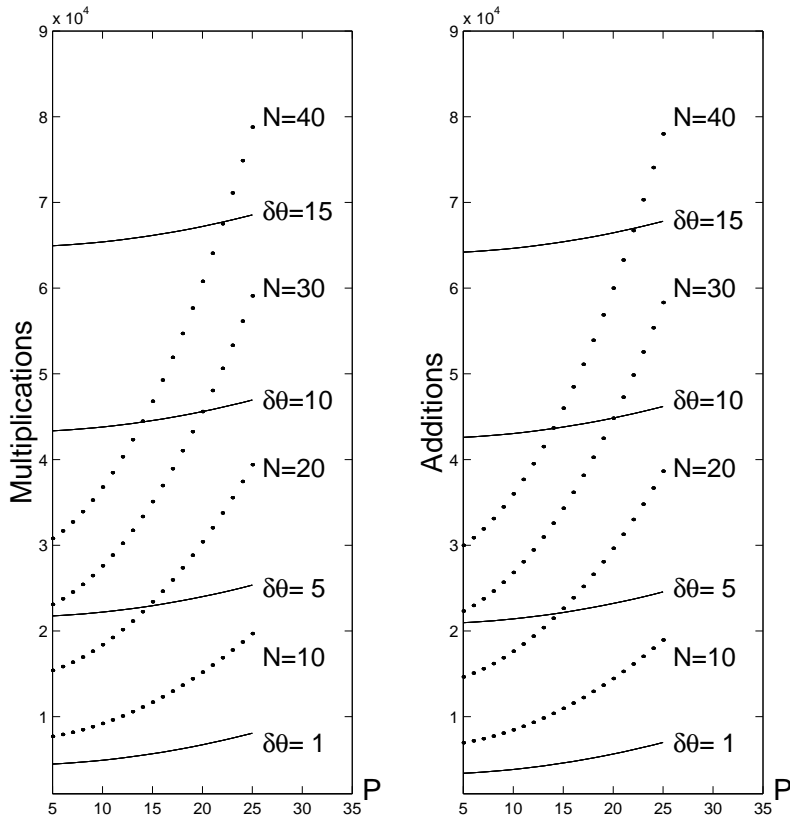
Figure 2: Complexity comparison between the exact steerability and the approximate steerability. The dotted curves represent the complexity of exactly steerable filters composed of N odd basis filters and N even basis filters with P as 1D tap size. The solid lines show the relation between complexity and the sampling interval $\delta\theta$ and P in computation of S and DS in our approach. We see that the approximate steerability is more efficient than the exact steerability, especially in the case of high orientation resolution and large filter size.

16
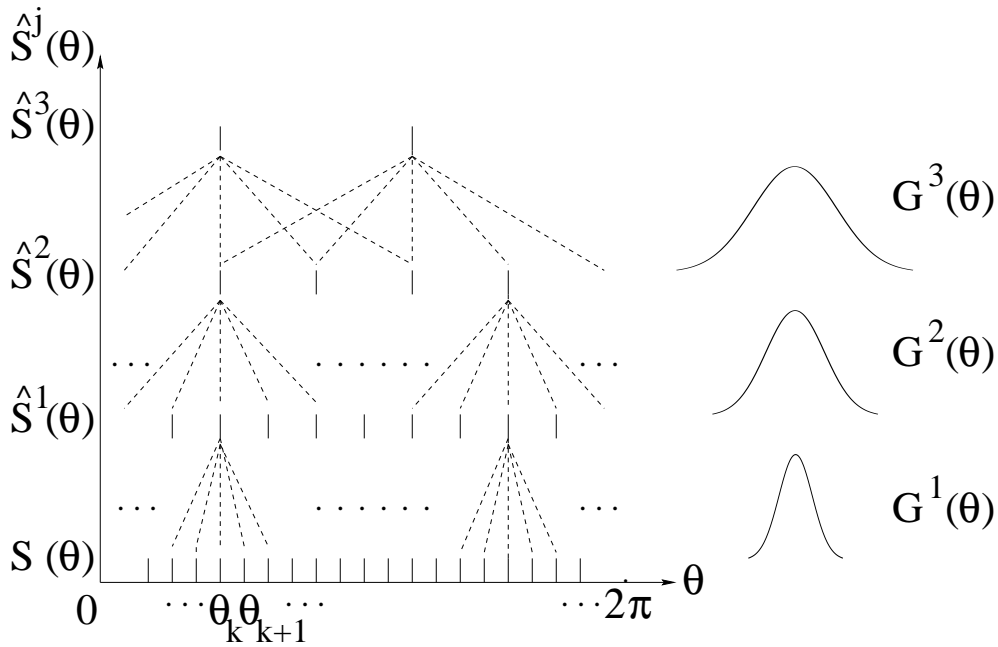
Figure 3: **Left:** Polar pyramid structure, $S(\theta)$ is the lowest level of the polar pyramid, namely the averaging outputs of sampling masks. $\hat{S}^j(\theta)(j = 1, 2, 3)$ are higher levels after subsampling with the generating kernel K_2 of equation (19). **Right:** Corresponding interpolation functions at different levels. They are Gaussian functions with different scales.
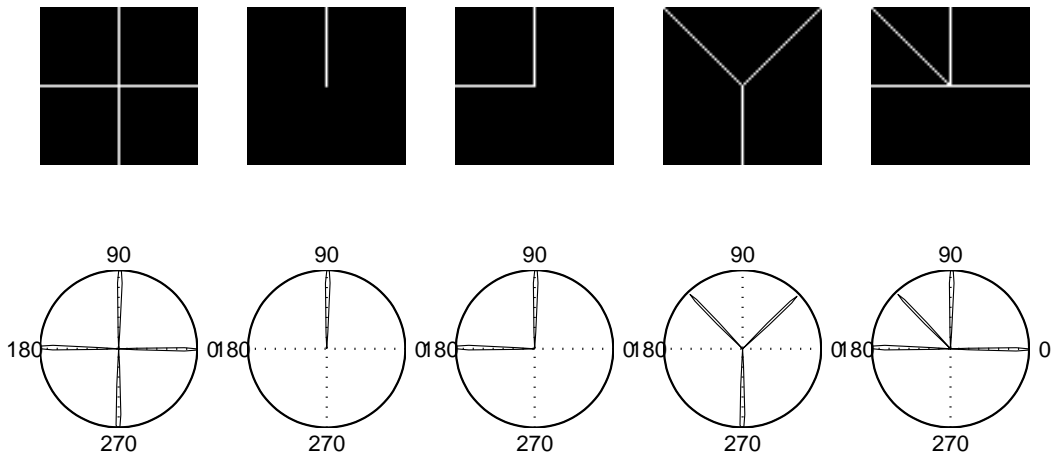
Figure 4: **Top:** Synthetic line junctions. **Bottom:** $S(\theta)$. $R_{\min} = 3, R_{\max} = 15$.

17
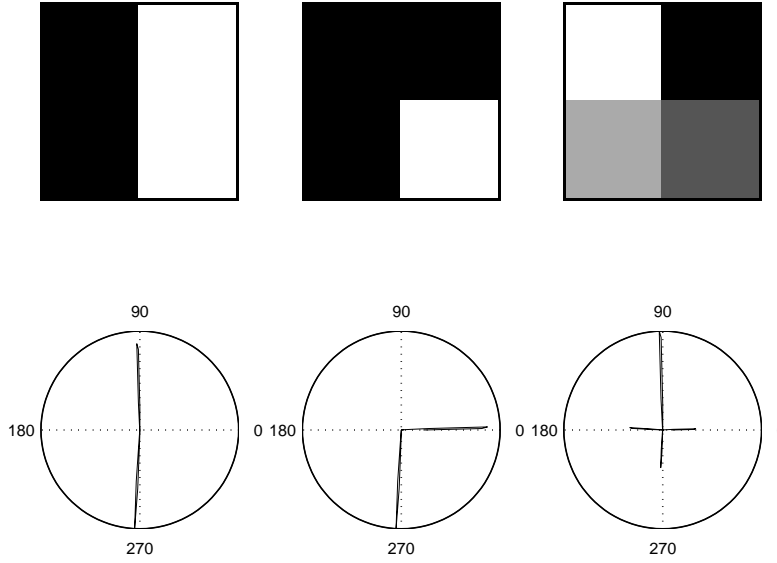
Figure 5: **Top:** Synthetic edge junctions. **Bottom:** $DS(\theta)$. The local maxima show the orientation of edges. $R_{\min} = 3$, $R_{\max} = 15$.
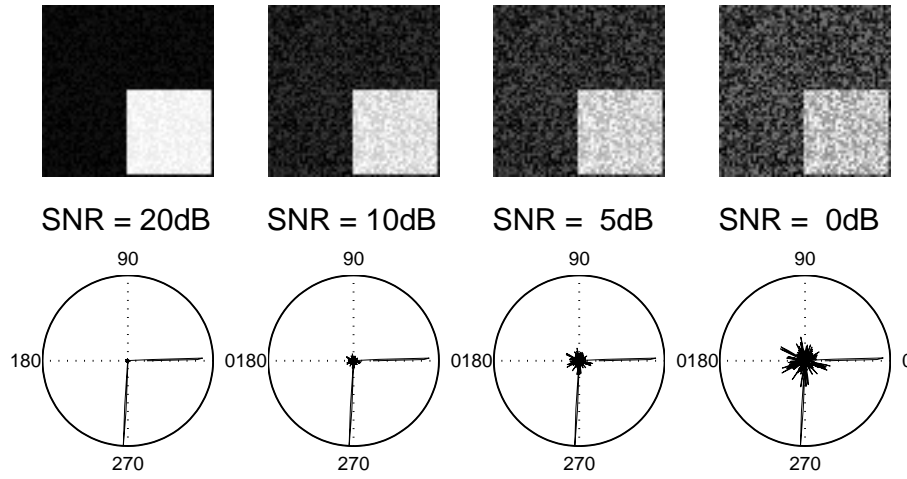
Figure 6: **Top:** A synthetic edge junction disturbed by four increasing levels of random noise. **Bottom:** Corresponding $DS(\theta)$. Even in the very noisy case ($\mathcal{SNR} = 0dB$) the signature can characterize the junction. $R_{\min} = 3$, $R_{\max} = 15$.
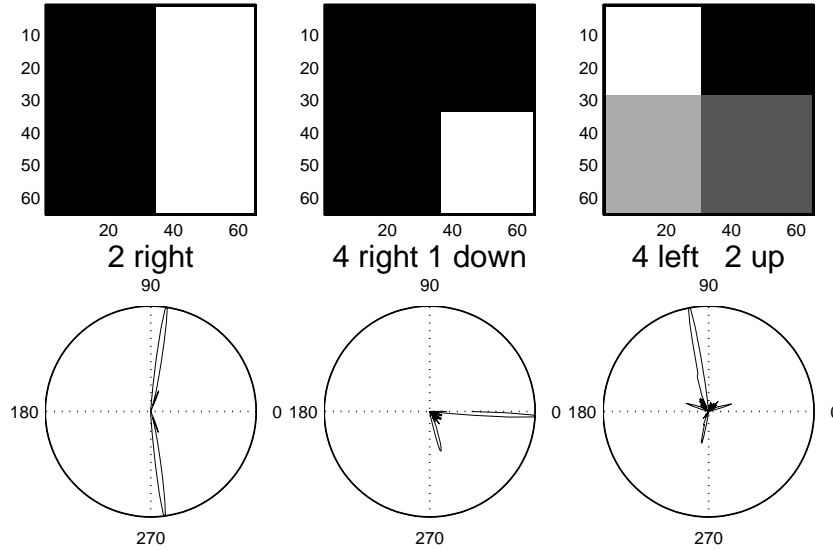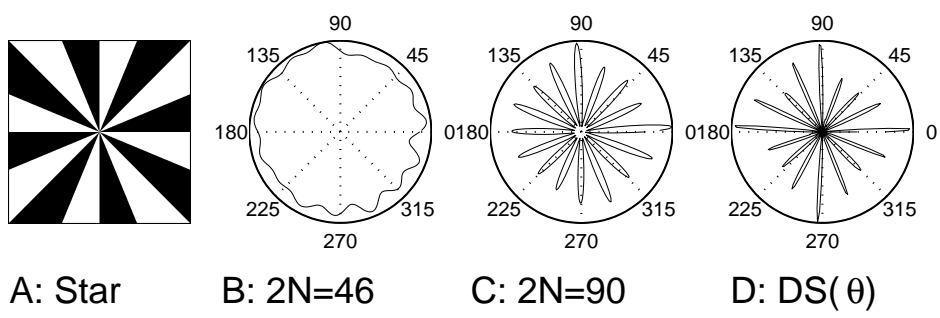
18

Figure 7: **Top:** Deviation of the keypoint from the central position of the mask. **Bottom:** $DS(\theta)$. $R_{\min} = 3, R_{\max} = 15$.

Figure 8: **A:** A "Siemens star" with 16 edges spanning uniformly the orientation space. **B:** Polar plot of the result using the steerable wedge filter [23] composed of 46 basis filters with 31-tap size. Totally 61486 multiplications and 60360 additions are needed. The edges are hardly discernible. **C:** The same as in **B** but using 90 basis filters with 119610 multiplications and 118440 additions. The orientations of the edges are clearly presented. **D:** $DS(\theta)$ using the Gaussian averaging steerable filter. We compute only 10086 multiplications and 9006 additions to achieve the same resolution.
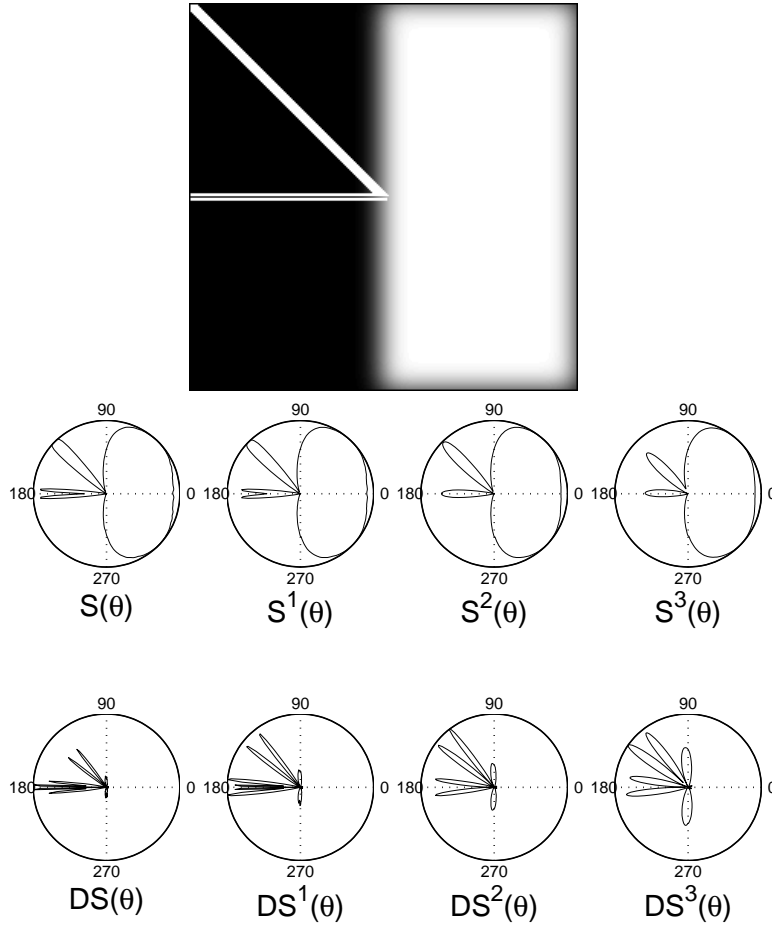
Figure 9: Characterizing a junction using the polar pyramid. **Top:** A junction composed of two close lines with distance of 1 pixel, two edges blurred by a Gaussian function with $\sigma = 4$ and a wide line with a width of 6 pixels. **Middle:** The characterizing signatures reconstructed from the first four levels of the polar pyramid: $S(\theta)$, $S^1(\theta)$, $S^2(\theta)$, and $S^3(\theta)$. The wide line is distinctly characterized in $S^3(\theta)$. But two close lines are also recognized as one line. **Bottom:** Corresponding $DS(\theta)$, $DS^1(\theta)$, $DS^2(\theta)$, and $DS^3(\theta)$. The blurred edges are presented more and more clearly with the increase of pyramid level. The neighboring boundaries of two close lines near $180°$ can be seen only at the first two levels. After increasing the scale only outer boundaries of these two lines are recognized.
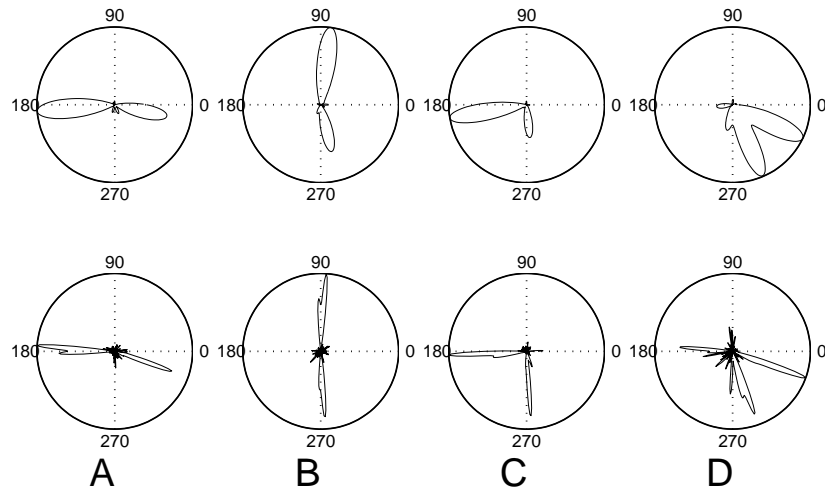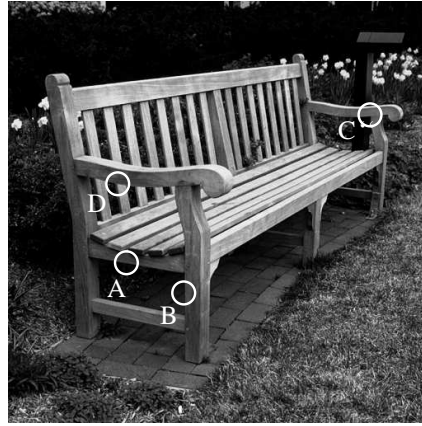
Figure 10: **Top:** The parkbench with marked edge junctions. **A**: horizontal edge; **B**: vertical edge; **C**: corner; **D**: 'T'-junction. **Middle:** Steerable wedge filter results using 30 basis filters. $P = 19$. **Bottom:** $DS(\theta)$ of the Gaussian averaging steerable filter. The edge near $180°$ in **D** is very blurred. But $DS(\theta)$ still can characterize it. $R_{\min} = 3, R_{\max} = 9$.
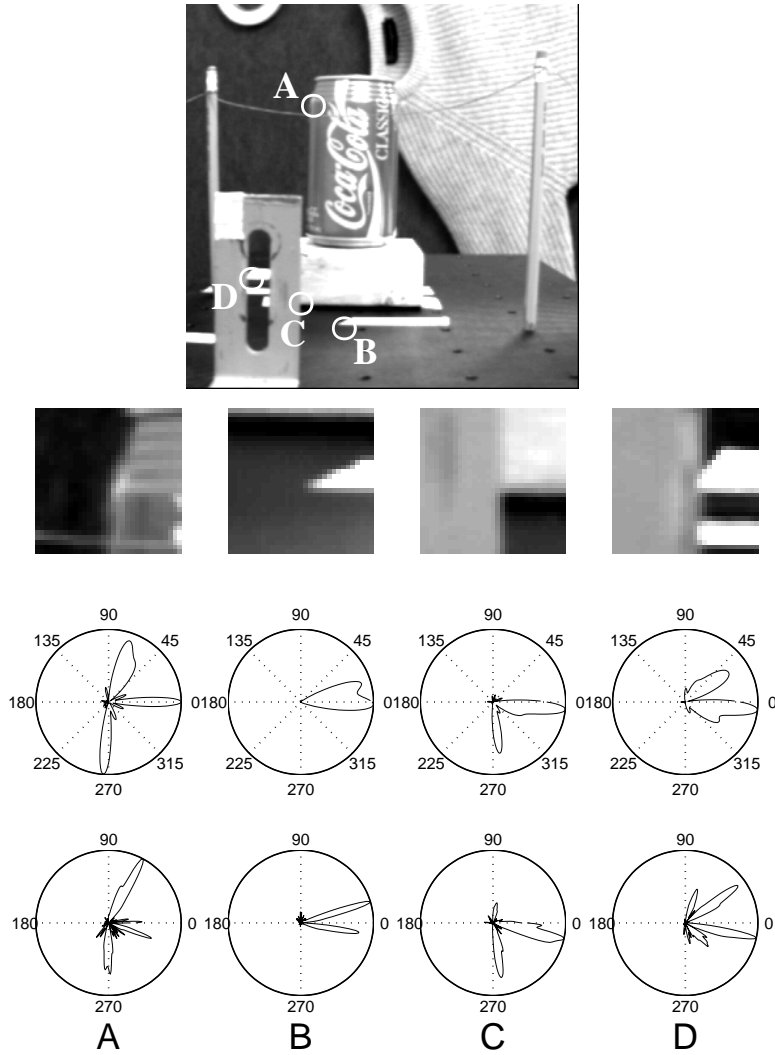
Figure 11: Comparison between the steerable wedge filter [23] and Gaussian averaging steerable filter. **Row 1:** An image of the NASA sequence with four kinds of marked junctions. **A**: 'Y' junction; **B**: 'V' junction; **C**: 'T' junction; **D**: 'K' junction. **Row 2:** Junctions in detail. The keypoints are not always at centers of the masks. **Row 3:** Polar plots using the steerable wedge filter [23] using 46 basis filters with 31 tap size. **Row 4:** $DS(\theta)$ using the Gaussian averaging steerable filter ($R_{\min} = 3, R_{\max} = 15$). Both methods are stable with respect to the offsets of keypoints. Our method presents higher orientation resolution with lower cost.
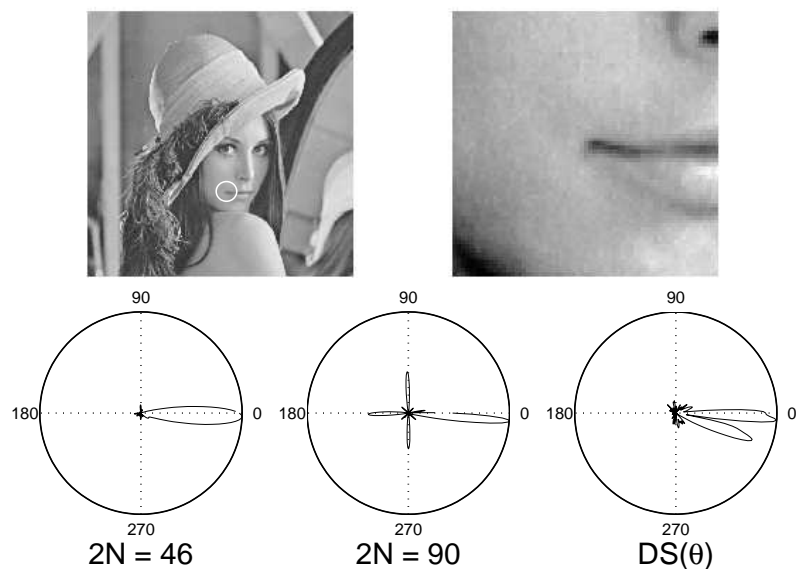
22

Figure 12: Resolution comparison between the steerable wedge filter [23] and the Gaussian averaging steerable filter. **Top Left:** The image "Lena" with her lips corner as a keypoint. **Top Right:** Lips corner in detail. **Bottom Left:** Polar plots using the steerable wedge filter [23] with 46 basis filters. Only the dominant dark line between the lips can be recognized. **Bottom Middle:** Even with 90 basis filters we cannot recognize two lips. **Bottom Right:** $DS(\theta)$ of the Gaussian averaging steerable filter. The edges of two lips are characterized distinctly.
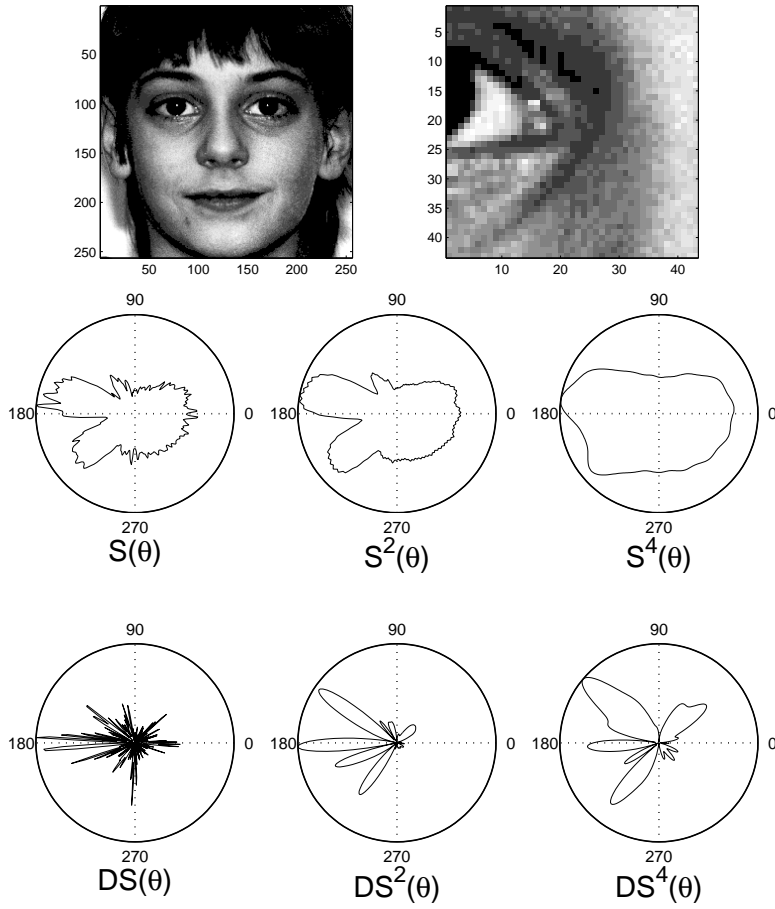
Figure 13: **Top Left:** Face of a child. **Top Right:** Its left eye corner in detail. It can be regarded as a combination of irregular wide lines and blurred edges disturbed by noise. **Middle:** Orientation signatures reconstructed from the first, third and fifth level of the polar pyramid. The eyelids are clear to see in $S^2(\theta)$ as two maxima at $135°$ and $225°$. The local maximum near $180°$ is due the white of the eye. **Bottom:** Corresponding $DS(\theta)$, $DS^2(\theta)$ and $DS^4(\theta)$. At small scales the signatures present more detail, but are also sensitive to noise. At large scales we obtain dominant structures but lose details. A valid characterization should combine all these signatures.

24

References

[1] E.P. Simoncelli, W.T. Freeman, E.H. Adelson and D.J. Heeger. Shiftable multi-scale transforms. *IEEE Trans. Information Theory*, 38(2):587–607, 1992.

[2] D. H. Ballard and L. E. Wixson. Object recognition using steerable filters at multiple scales. In *IEEE Workshop on Qualitative Vision*, pages 2–10, 1993.

[3] J. Babaud , A. P. Witkin , M. Baudin and R. O. Duda. Uniqueness of the Gaussian kernel for scale-space filtering. *IEEE Trans. Pattern Analysis and Machine Intelligence*, 8:26–33, 1986.

[4] W. Beil. Steerable filters and invariance theory. *Pattern Recognition Letters*, 15:453–460, 1994.

[5] R. N. Bracewell. *The Fourier Transform and Its Applications*. McGraw-Hill Book Company, 1986.

[6] P. J. Burt and E. H. Adelson. The Laplacian pyramid as a compact image code. *IEEE Transactions on Communications*, 31:532–540, 1983.

[7] P.-E. Danielsson. Rotation-invariant linear operators with directional response. In *Proc. Int. Conf. on Pattern Recognition*, Miami, Dec., 1980.

[8] J. G. Daugman. Uncertainty relation for resolution in space, spatial frequency and orientation optimized by two-dimensional visual cortical filters. *Journal of the Optical Society of America*, 2(7):1160–1169, 1985.

[9] W. Foerstner. A framework for low level feature extraction. In *Proc. Third European Conference on Computer Vision*, volume II, pages 383–394, Stockholm, Sweden, May 2-6, J.O. Eklundh (Ed.), Springer LNCS 801, 1994.

[10] W.T. Freeman and E.H. Adelson. The design and use of steerable filters. *IEEE Trans. Pattern Analysis and Machine Intelligence*, 13:891–906, 1991.

[11] L. Parida, D. Geiger and R. Hummel. Junctions: Detection, classification, and reconstruction. *IEEE Trans. Pattern Analysis and Machine Intelligence*, 20(7):687–698, 1998.

[12] G. Sommer, M. Michaelis, R. Herpers. The SVD approach for steerable filter design. In *IEEE International Symposium on Circuits and Systems*, volume V, pages 349–353, Monterey, CA, May 31-June 3, 1998.

[13] H. Knutsson and G. H. Granlund. Texture analysis using two-dimensional quadrature filters. In *IEEE Comput. Soc. Workshop Comp. Architecture Patt. Anal. Image Database Mgmt.*, pages 388–397, 1983.

[14] M. Michaelis. *Low level image processing using steerable filters*. PhD thesis, Institute of Computer Science, University Kiel, Germany, 1995. also available as Tech. Report No. 9716.

[15] M. Michaelis and G. Sommer. Junction classification by multiple orientation detection. In *Proc. Third European Conference on Computer Vision*, volume I, pages 101–108, Stockholm, Sweden, May 2-6, J.O. Eklundh (Ed.), Springer LNCS 800, 1994.

[16] M. Michaelis and G. Sommer. A Lie group approach to steerable filters. *Pattern Recognition Letters*, 16:1165–1174, 1995.

[17] V. S. Nalwa. *A Guided Tour of Computer Vision*. Addison-Wesley Publishing Company, 1993.

[18] A.V. Oppenheim and R.W. Schafer. *Digital Signal Processing*. Prentice-Hall, Inc., 1975.

[19] P. Perona. Steerable-scalable kernels for edge detection and junction analysis. *Image and Vision Computing*, 10(10):663–672, 1992.

[20] P. Perona. Deformable kernels for early vision. *IEEE Trans. Pattern Analysis and Machine Intelligence*, 17(5):488–499, 1995.

[21] K. Rohr. Recognizing corners by fitting parametric models. *International Journal of Computer Vision*, 9(3):213–230, 1992.

[22] K. Rohr. On the precision in estimating the location of edges and corners. *Journal of Mathematical Imaging and Vision*, 7:7–22, 1997.

[23] E. P. Simoncelli and H. Farid. Steerable wedge filters for local orientation analysis. *IEEE Trans. Image Processing*, 5(9):1377–1382, 1996.

[24] P.C. Teo and Y. Hel Or. Lie generators for computing steerable functions. *Pattern Recognition Letters*, 19(1):7–17, 1998.